

Modelling the Lift Crisis of a Cambered Plate at 0° Angle of Attack

S. Nava¹, P. Bot², J. Cater³ and S. E. Norris¹

¹Department of Mechanical Engineering
University of Auckland, Auckland 1142, New Zealand

²Naval Academy Research Institute
Lanveoc, Brest 29240, France

³Department of Engineering Science
University of Auckland, Auckland 1142, New Zealand

Abstract

Water tunnel experiments have shown that the lift of a cambered plate at zero degrees angle of attack undergoes a sudden change in sign at a critical Reynolds number. This has been experimentally determined as approximately 2×10^5 and PIV measurements reveal the change in the lift to be associated with the sudden reduction in size of the region of separated flow at the trailing edge. In order to understand the flow, the physical experiment has been modelled using the Reynolds-Averaged Navier-Stokes (RANS) equations and Large Eddy Simulation (LES). Both modelling methods predicted the change in sign of the lift, but the RANS solutions did not predict the sudden change in sign. However the LES model successfully reproduced this behaviour.

Introduction

The *Drag Crisis* is the sudden decrease in drag experienced by bluff bodies such as cylinders, when the Reynolds number increases above some critical value. At low Reynolds numbers the boundary layer at the front of the body is laminar, which readily separates forming a broad wake. However, above a critical Reynolds number the boundary layer transitions to turbulence before the laminar separation point. The turbulent boundary layer is more resistant to separation and separates later, resulting in a decrease in the size of the separated region and a reduction in the pressure drag on the body[2, 4, 9].

Recent experiments in the water tunnel at the French Naval Academy Research Institute at Brest (IRENav)[5, 1] have revealed similar behaviour for the lift of the highly-cambered circular arc aerofoil shown in Figure 1. At 0° angle of attack the aerofoil generates a negative lift at low Reynolds numbers, with the flow separating from the convex upper surface at the mid-chord. However, above a critical Reynolds number the flow becomes attached to the trailing edge, and the lift changes sign becoming positive. This has been named the *Lift Crisis* from its similarity to the Drag crisis.

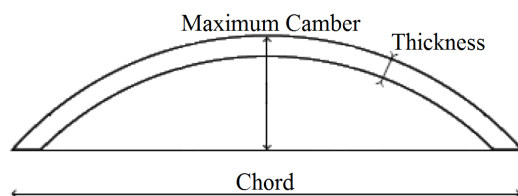


Figure 1: The profile of the circular arc foil. From [5]

Even though a circular arc in uniform flow is geometrically simple with well defined boundary conditions, modelling the change in flow structure due to the lift crisis is a challenging test case for numerical methods.

Haase et al.[3] reported the results of a series of studies that tested different RANS models, LES, and hybrid methods such as Detached Eddy Simulation (DES) on a series of benchmark cases. They showed that the flow was more accurately predicted by the DES and LES models, especially in case of substantial flow separation. Roberts & Yaras[8] showed excellent agreement between LES and experiments in the prediction of the boundary layer transition in a laminar separation bubble. The predictive performance of LES was tested by Mittal et al.[7] who simulated the flow through a low-pressure turbine cascade. Their model successfully predicted the different trailing edge separation structures that occurred for different Reynolds numbers.

This suggests that LES should be able to predict the transition and separation processes that cause the sudden change in the lift of the foil, while RANS methods that do not account for transition would not be expected to predict these flows. However, the $\gamma - \theta$ modification of the SST RANS turbulence model[6] has been developed to model transition in boundary layers, and may be able to model the lift crisis. In this paper we examine how well these models are able to model the lift crisis.

Experimental Methodology

The experiments were performed in the IRENav water tunnel in Brest in France shown in Figure 2. The tunnel is fitted with a force balance and a PIV flow measurement system within the $192 \text{ mm} \times 192 \text{ mm}$ cross section test section, which is 1 m long and is located downstream of a flow calming honeycomb section and a $1/9$ contraction as shown in Figure 3.

The tested foil was a 3 mm-thick, 50 mm-radius stainless steel circular arc. The resulting section had a chord length of 74.4 mm and a maximum camber of 16.6 mm located at mid-chord, as shown in Figure 1. The cambered plate spanned the full width of the test section with a small gap at each end to avoid contact with the tunnel walls. It could be rotated to achieve a range of angles of attack, but only results for 0° are presented here. The experiment was carried out at different flow speeds, with the onset flow velocity varying between 0.93 m/s and 8.13 m/s, corresponding to a range of Reynolds numbers between 0.7×10^5 and 6×10^5 . The measured turbulence intensity was 1.8 % at the model location.

Forces were recorded at 1 kHz frequency and time-averaged over a period of 30 seconds. The velocity field was measured using a PIV system, with 300 image pairs recorded on a plane at the mid-span of the foil at a frequency of 10 Hz. The flow

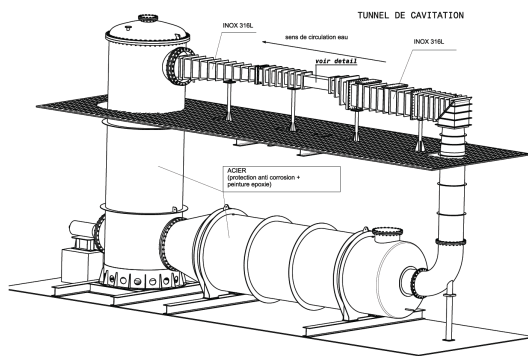


Figure 2: Layout of the IRENav water tunnel at Brest. Adapted from [5]

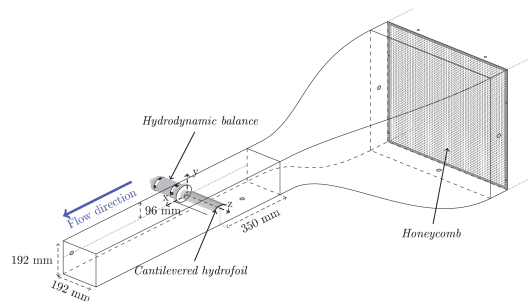


Figure 3: The test section of the IRENav water tunnel. Adapted from [5]

field was averaged using the entire set of image pairs.

Numerical Methodology

The flow around the arc was modelled using both RANS and LES. The 1 m long test section of the water tunnel was reproduced in the computational model with the circular arc placed approximately 4 chordlengths downstream of the inlet. The inlet was modelled with a prescribed uniform inlet velocity, while the outlet had a constant pressure. The upper and lower walls were modelled as free-slip walls.

The mesh used is shown in Figure 4 and was a H-type block-structured mesh which was generated using ICM-CFD. On the foil the chordwise cell dimension varied from $10 \mu\text{m}$ at the leading edge to $100 \mu\text{m}$ at the trailing edge with a maximum size of $400 \mu\text{m}$ at the mid-chord. The cells had a thickness of $5 \mu\text{m}$ normal to the wall, which ensured a maximum y^+ value of ≤ 1 . For the RANS calculations the flow was modelled as two dimensional on a mesh that was one cell thick. For the LES calculations the mesh had 18 equispaced points in the spanwise direction, with a width of $c/4$, where c is the length of the chord, and periodic boundary conditions were applied in the spanwise direction.

The RANS calculations were made using ANSYS CFX using the Barth-Jespersion “High Resolution” differencing scheme for the momentum and the turbulence scalars. Steady and unsteady RANS calculations were made, but the unsteady simulations converged to steady state. Both the standard SST and the γ - θ -SST[6] turbulence models were used, the latter model having a correction to account for boundary layer transition. A 1.5%

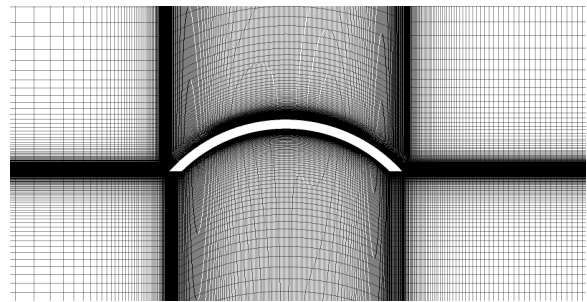


Figure 4: Longitudinal section of the mesh around the circular arc.

turbulence intensity was used at the inlet with a length scale of 0.01 m.

ANSYS Fluent was used for the LES calculations with a second-order fractional time stepping scheme, which used an Adams-Bashforth scheme used for the momentum terms and Crank-Nicolson differencing for the diffusion. The timestep was such that the Courant number was lower than 1 throughout the domain. The momentum equations were discretised with second order central differences, and the dynamic Smagorinsky-Lilly subgrid scale model was used. The inlet flow turbulence intensity was 0.5% with a turbulence length scale of 0.1 m. The results were averaged over a period of approximately 30 pass-throughs, where the pass-through time was calculated as the ratio between the chordlength and the onset velocity. The averaging period started after an initial period of 15 pass-throughs to allow the flow field to develop.

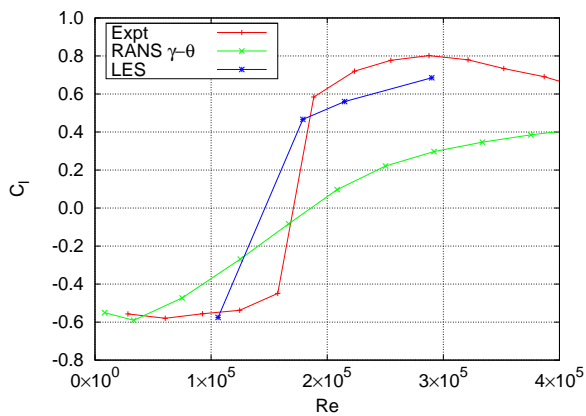
The calculations were performed on an Intel based computational cluster with an infiniband interconnect, and the wallclock times for RANS calculations varied between 1 to 2 hours using 24 cores while LES calculations took approximately 200 hours using 128 cores.

Results and Discussion

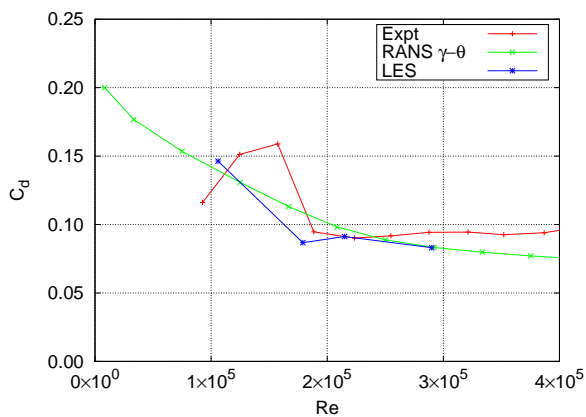
The flow was calculated for sixteen different Reynolds numbers using RANS, but due to the computational cost only four different Reynolds numbers were simulated using LES, two on either side of the expected change in sign of the lift.

The computed lift coefficients for the foil are shown in Figure 5 and compared with experiment. Based on the assumption that the lift crisis is due to transition, it would be expected that the RANS solutions calculated with the standard SST model would not predict the change in sign of the lift. This was indeed the case and so the results have been omitted for clarity. The RANS solutions calculated using the γ - θ model are shown, and the method does predict the reversal in the direction of lift. However, it does not have the discontinuous change seen in the experimental values, but instead exhibits a gradual continuous change in values from negative to positive over the Reynolds number range of 2×10^4 to 3×10^5 . From the limited LES data available it appears that LES succeeded in modelling the sharp change of sign of the lift coefficient although the critical Reynolds number differs from the experiment. The computational results located the lift jump around 1.5×10^5 , with the computed lift coefficient changing from -0.58 to 0.48 matching the experimental data. Both the RANS and the LES data show a systematic underestimation of the lift coefficient at high Reynolds numbers, although the predicted trend is correct.

The experimental drag coefficient undergoes a drop across the



(a) Lift coefficient



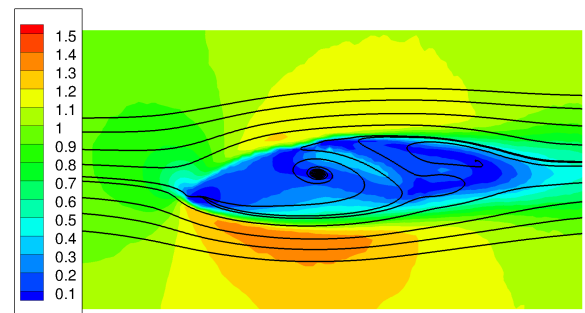
(b) Drag coefficient

Figure 5: Variation of (a) lift and (b) drag coefficient with Reynolds number; computed data compared with experiment.

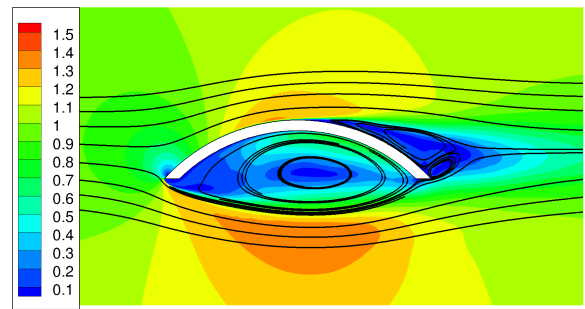
critical Reynolds number which was matched by the computational models. As with the lift coefficient, the LES model predicted a sudden change in the value of the drag coefficient. The γ - θ RANS solutions gave a smooth transition between the low and high-Reynolds number behaviour.

Figures 6 and 7 illustrate the phenomena behind the change in the direction of the lift force and the magnitude of the drag coefficient. The low Reynolds number flow is shown in Figure 6a. The PIV and LES data is shown for $Re=1.1 \times 10^5$, but the RANS data is shown at a lower Reynolds number of $Re=3.3 \times 10^4$ at which it has a similar lift coefficient as the PIV and LES data. The flow over the upper surface is separated from the mid-chord to the trailing edge. A strong recirculating flow occupies the cavity on the lower surface, and has a rounded lower boundary that accelerates the flow under the foil. The combination of these two factors result in a negative lift coefficient, while the separation on the upper surface acts to increase the drag coefficient.

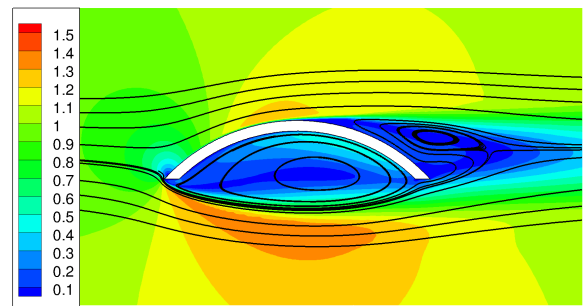
Once the Reynolds number exceeds the critical value, the boundary layer on the upper face of the cambered plate undergoes a transition from laminar to turbulent flow and remains attached to the trailing edge. Figure 7a shows this flow for $Re=2.9 \times 10^5$ for the PIV and LES data, and $Re=4.2 \times 10^5$ for the RANS. The region of separation on the upper surface is reduced in size, and the recirculation in the lower cavity is not as strong and does not extend downwards into the flow. The attached flow on the upper surface results in a higher lift coefficient and reduced drag.



(a) PIV: $Re=1.1 \times 10^5$.



(b) LES: $Re=1.1 \times 10^5$.



(c) RANS: γ - θ $Re=3.3 \times 10^4$.

Figure 6: Comparison of experimental and computed flow fields at subcritical Reynolds numbers. Streamlines and contours of U/U_{inlet} .

cient and reduced drag.

Figures 6a, 6b and 6c show that both the LES and RANS γ - θ CFD models have accurately predicted the location of the stagnation point on the upper surface of the plate, just downstream of the leading edge. All have the flow separating from the upper surface at the mid-chord, although the LES data seems to have a shorter wake than the PIV (and RANS) data.

Figure 7 shows reasonable agreement between the PIV and the LES and RANS CFD predictions for the high Reynolds number case. The separation point on the convex upper surface has moved downstream compared to the low Reynolds and there is reduced trailing edge separation. It should be noted that the LES and RANS solutions have a larger region of trailing edge separation than occurs in the experiment, which results in the lower values of the predicted lift coefficients. This is particularly true for the RANS solution. It is unclear if this is due to the turbulence models used with the RANS and LES predictions, or due to the computed flows neglecting the interaction between the plate and the side walls of the water tunnel.

The transition of the boundary layer on the upper surface of the curved plate is illustrated in Figure 8 which shows the turbulent

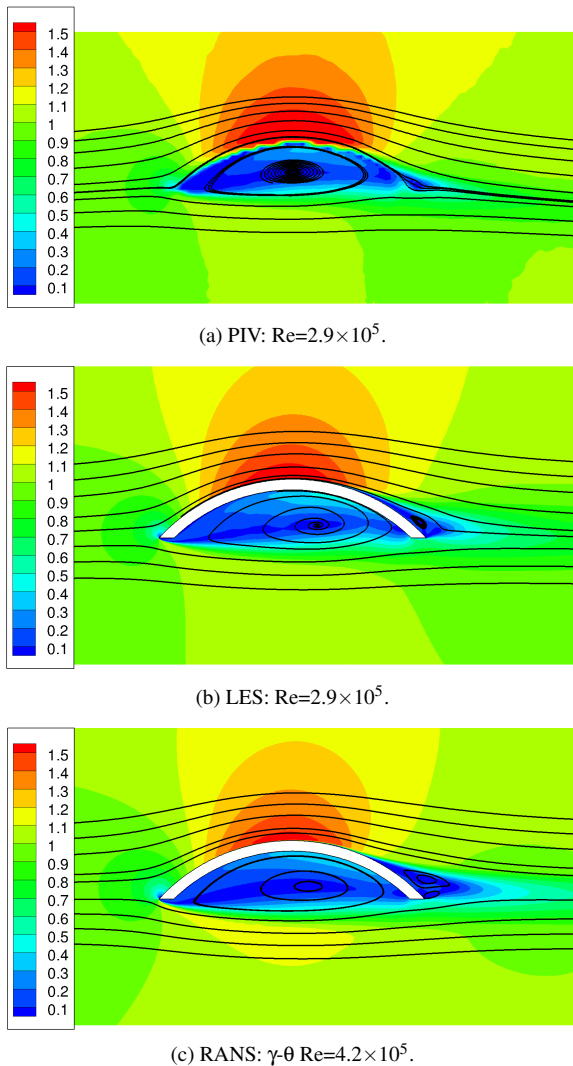


Figure 7: Comparison of experimental and computed flow fields at supercritical Reynolds numbers. Streamlines and contours of U/U_{inlet} .

intermittency calculated by the RANS $\gamma\text{-}\theta$ model. The boundary layer flow on the upstream half of the plate is laminar and has a low intermittency. At low Reynolds numbers the boundary layer separates from the foil and transitions to turbulent well away from the foils surface. However, at high Reynolds numbers the boundary layer becomes turbulent (the intermittency $\gamma = 1$) and remains attached. Careful examination of the figure reveals that transition occurs in a laminar separation bubble. Unfortunately, the PIV data is unable to reveal if this occurs, and the experimental foil is not pressure tapped, so it is unknown if this occurs in practice.

Conclusions

Experiments of the hydrodynamics of a curved plate have revealed that the lift and drag force are strongly dependant on the Reynolds number. At low Reynolds numbers the flow is dominated by the separation of the laminar boundary from the convex surface, resulting in a large separated region giving rise to a negative lift force and comparatively large drag coefficient. As the Reynolds number increases beyond a critical value the separated flow reattaches, the lift force becomes positive, and the drag coefficient drops.

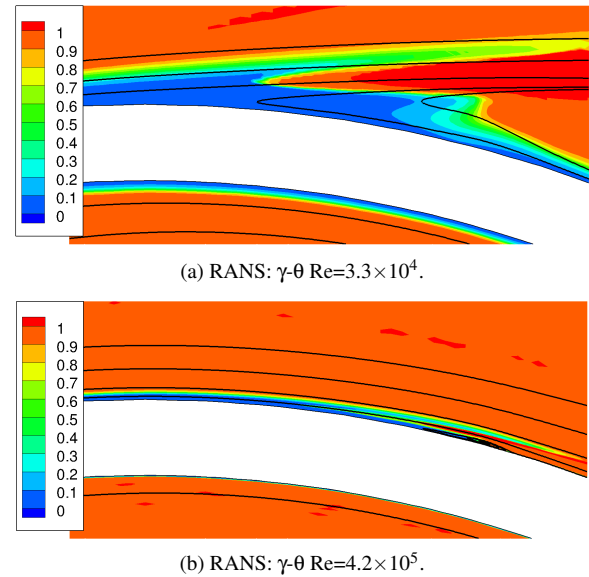


Figure 8: Plot of the turbulent intermittency calculated by the RANS $\gamma\text{-}\theta$ model, on the mid-chord of the curved plate.

The LES and RANS $\gamma\text{-}\theta$ models predicted both the low and high-Reynolds numbers flows. The LES model proved capable of modelling the sudden transition at the critical Reynolds number. The RANS solution incorrectly predicted a gradual continuous change between the low and High Reynolds number flows.

References

- [1] Bot P., Rabaud M., Thomas G., Lombardi A. & Lebret C., Sharp transition in the lift force of a fluid flowing past non-symmetrical obstacles: Evidence for a lift crisis in the drag crisis regime *Physical Review Letters*, in press.
- [2] Delany N.K. & Sorensen N.E., *Low-speed drag of cylinders of various shapes*, NACA Technical Note 3038, 1953.
- [3] Haase W., Braza M. & Revell A., *DESider-A European effort on hybrid RANS-LES modelling*, Springer, 2009.
- [4] Landau L.D., & Lifchitz E.M., *Fluid Mechanics*, Pergamon, 1963.
- [5] Lombardi, A., *Experimental Analysis of a Highly Cambered Thin Profile*, MSc Thesis, University of Strathclyde, 2014.
- [6] Menter, F.R., Langtry, R., Likki, S., Suzen, Y., Huang, P. & Völker, S., A correlation-based transition model using local variables—Part I: model formulation, *Journal of Turbomachinery*, **128**, 2006, 413-422.
- [7] Mittal R., Venkatasubramanian S. & Najjar F.M., Large-Eddy Simulation of flow through a low pressure turbine cascade, in *15th AIAA Computational Fluid Dynamics conference*, Anaheim, California, June 11-14, 2001.
- [8] Roberts S.K. & Yaras M.I., Large-Eddy Simulation of transition in a separation bubble, *Journal of Fluids Engineering*, **182**, 2005, 232-238.
- [9] Singh S.P. & Mittal S., Flow past a cylinder: shear layer instability and drag crisis, *International Journal for Numerical Methods in Fluids*, **47**, 2005, 75-98.